Acta Pharmaceutica Sinica B 2025;15(6):3226−3242

Chinese Pharmaceutical Association
Institute of Materia Medica, Chinese Academy of Medical Sciences

Acta Pharmaceutica Sinica B

www.elsevier.com/locate/apsb
www.sciencedirect.com

ORIGINAL ARTICLE

Targeting stem-property and vasculogenic mimicry for sensitizing paclitaxel therapy of triple-negative breast cancer by biomimetic codelivery

Siqi Wu[a,b], Qing Tang[c], Weifeng Fang[d], Zhe Sun[a], Meng Zhang[e], Ergang Liu[b], Yang Cao[a,*], Yongzhuo Huang[a,b,d,f,*]

[a]*Department of Oncology, the First Affiliated Hospital and the First Clinical School of Guangzhou University of Chinese Medicine, Guangzhou 510000, China*
[b]*Zhongshan Institute for Drug Discovery, Shanghai Institute of Materia Medica, Chinese Academy of Sciences, Zhongshan 528400, China*
[c]*State Key Laboratory of Traditional Chinese Medicine Syndrome, Clinical and Basic Research Team of TCM Prevention and Treatment of NSCLC, Guangdong Provincial Hospital of Chinese Medicine, the Second Clinical College of Guangzhou University of Chinese Medicine, Guangzhou 510000, China*
[d]*School of Chinese Materia Medica, Nanjing University of Chinese Medicine, Nanjing 210023, China*
[e]*Department of Pharmacy, Women's Hospital, Zhejiang University School of Medicine, Hangzhou 310006, China*
[f]*State Key Laboratory of Drug Research, Shanghai Institute of Materia Medica, Chinese Academy of Sciences, Shanghai 201203, China*

Received 15 December 2024; received in revised form 20 February 2025; accepted 22 February 2025

KEY WORDS

Shikonin;
Paclitaxel;
Triple-negative breast cancer;
Pyruvate kinase M2 (PKM2);
Cancer stem-like cells;
Vasculogenic mimicry;

Abstract Triple-negative breast cancer (TNBC) is aggressive, with high recurrence rates and poor prognosis. Paclitaxel (PTX) remains a key chemotherapeutic agent for TNBC, but its efficacy diminishes due to the emergence of drug resistance, largely driven by cancer stem-like cells (CSCs), vasculogenic mimicry (VM) formation and tumor immunosuppressive microenvironment (TIME). Pyruvate kinase M2 (PKM2) is highly expressed in TNBC, and is a potential target for TNBC treatment. In this study, we developed a biomimetic codelivery system using albumin nanoparticles (termed S/P NP) to co-encapsulate PTX and shikonin (SHK), a natural inhibitor of PKM2. By inhibiting PKM2, SHK suppressed β-Catenin signaling, thereby reversing CSC stemness and preventing VM formation. The S/P NP system exhibited tumor-targeting delivery effect and significantly inhibited TNBC growth and lung

*Corresponding authors.
E-mail addresses: caoyang0342@gzucm.edu.cn (Yang Cao), yzhuang@simm.ac.cn (Yongzhuo Huang).

Peer review under the responsibility of Chinese Pharmaceutical Association and Institute of Materia Medica, Chinese Academy of Medical Sciences.

https://doi.org/10.1016/j.apsb.2025.04.006

Tumor microenvironment; Albumin

metastasis. Mechanistically, the treatment reversed epithelial−mesenchymal transition (EMT) and stem-like properties of TNBC cells, suppressed VM formation, and remodeled the TIME. It reduced immunosuppressive cells (M2 macrophages, MDSCs) while promoting anti-tumor immunity (M1 macrophages, dendritic cells, cytotoxic T cells, and memory T cells). This dual-action strategy holds promise for improving TNBC therapy by targeting CSCs, VM, and the immune microenvironment, and for overcoming PTX resistance and reducing metastasis.

1. Introduction

Triple-negative breast cancer (TNBC) is characterized by high invasiveness, proneness to relapse, and poor prognosis[1,2]. Paclitaxel (PTX) is a mainstay of TNBC treatment. However, a wealth of clinical and experimental evidence indicates that PTX alone is insufficiently effective against TNBC, with significantly decreased efficacy after repeated administration[3,4]. Consequently, the conventional and classic TNBC treatment usually combines PTX with other chemotherapeutic drugs[5], immune checkpoint blockade[6], or anti-angiogenic therapies[7]. To sensitize PTX treatment and to seek an efficient and affordable combination therapy are important for improving TNBC treatment.

Cancer stem-like cells (CSCs) have been identified as a major factor in the poor response to PTX therapy and cancer recurrence in breast cancer (BC)[8], which is attributed to their capacity for self-renewal and production of heterogeneous cell lineages[9,10]. CSCs, characterized as a typical undifferentiated cancer cell phenotype, are rich in poorly differentiated tumors, which are linked to high-grade malignancy and poor prognosis compared to well-differentiated tumors[11,12]. Vasculogenic mimicry (VM) is a specific type of vasculature formation characterized by endothelial-like tumor cells themselves constituting the tubular structures that acts as pseudo blood vessels; VM is an important mechanism for poor response to PTX therapy[13,14]. VM is an alternative means to transport oxygen and nutrients to tumor cells[15], which is linked to poor overall survival (OS) in patients, thus being a viable therapy target[16-18]. Notably, CSCs and VM are closely associated with each other. CSCs lose some epithelial properties and gain endothelial-like cell characteristics that contribute to VM formation[19]. Specifically, CSCs inside TNBC can form VM, serving as its source[20]. On the other hand, the process of VM can maintain stemness characteristics of cancer cells[21]. Importantly, factors such as hypoxia can upregulate the genes associated with both CSC properties and VM, creating a feedback loop to promote tumor aggressiveness[22]. It is a widely-accepted paradigm that there is a close link between CSCs, VM and tumor immunosuppressive microenvironment (TIME).

Pyruvate kinase M2 (PKM2) is a crucial target involved in the stem-property of cancer cells[23], VM formation[24] and TIME[25]. The tetramer of PKM2 is a crucial enzyme that controls glycolysis rate[26]. By contrast, the dimeric PKM2 performs its nonmetabolic functions *via* translocation into nucleus, where PKM2 binds with β-Catenin, leading to the activation of β-Catenin signaling pathway[27]. Notably, this pathway plays a vital role in maintaining the stem property of CSCs by promoting their renewal, proliferation, and differentiation[28]. It, in turn, makes the cancer cell resistant to PTX and other chemotherapeutic drugs[29]. Therefore, the inhibition of PKM2 is expected to decrease the stem-property of cancer cells and the formation of VM, and remodel TIME, leading to re-sensitization of PTX therapy.

Herein, we proposed a PKM2 inhibition strategy for simultaneously blocking the cytoplasmic tetramer PKM2 to inhibit lactate production, as well as the nuclear ectopic of dimeric PKM2 to deactivate β-Catenin. By this way, it is expected that the stem-property of cancer cells and the formation of VM could be reversed, and TIME remodeled, leading to re-sensitization of PTX therapy. Shikonin (SHK), a naturally sourced naphthoquinone compound, is a classic PKM2 inhibitor with potent anticancer activity[30]. In our study, an albumin-based nanoparticulate system was developed for codelivery of SHK and PTX (S/P NP) for synergistic therapy. Albumin is a main nutritional source for tumors, which primarily targets the albumin-binding proteins (such as SPARC) that are overexpressed in tumor cells and tumor vasculature, thus serving as an ideal drug carrier[31-34].

2. Materials and methods

2.1. Materials

Shikonin (SHK) was purchased from Woge Dongfang Biotechnology Co., Ltd. (Beijing, China). Paclitaxel (PTX) was purchased from Shaoyuan Biotechnology Co., Ltd. (Shanghai, China). Lecithin was purchased from Yuanye Biotechnology Co., Ltd. (Shanghai, China). Bovine serum albumin (BSA) was purchased from Aladdin Bio-chem technology Co., Ltd. (Shanghai, China). RPMI-1640 medium, fetal bovine serum (FBS) were purchased from Dalian Meilun Biotechnology Co., Ltd. (Dalian, China). Cell Counting Kit-8 (CCK8) was purchased from GLPBIO (Montclair, USA). Cy5.5 was purchased from MedChemExpress LLC (NJ, USA). Collagenase IV and hyaluronidase were purchased from Biosharp (Beijing, China). The Total RNA Isolation Kit was purchased from FOREGENE (Chengdu, China). PKM2 antibody, SOX2 antibody, OCT4 antibody, vimentin antibody, E-cadherin antibody, β-tubulin antibody, CDH5 antibody were purchased from Abmart (Shanghai, China). β-Catenin antibody, GAPDH antibody were purchased from Abcam (Cambridge, UK). VEGFA antibody was purchased from Abclonal (Wuhan, China). Calreticulin monoclonal antibody (Alexa Fluor 488 conjugate), Alexa Fluor 488 conjugated goat anti-rabbit secondary antibody, HRP-conjugated Affinipure goat anti-mouse IgG, HRP-conjugated Affinipure goat anti-rabbit IgG were purchased from Proteintech (Wuhan, China). Recombinant murine macrophage colony-stimulating factor (M-CSF), granulocyte-macrophage colony-stimulating factor (GM-CSF), interferon-gamma (IFN-γ), and

interleukin-4 (IL-4) were obtained from Peprotech (NJ, USA). cDNA synthesis SuperMix kit, qPCR SYBR® Green Master Mix, Matrigel Basement Membrane Matrix were purchased from Yeasen Biotechnology Co., Ltd. (Shanghai, China). Mouse HMGB-1 ELISA Kit was purchased from Chenglin Huihuang Biotechnology Co., Ltd. (Beijing, China). ATP Assay Kit was purchased from Beyotime Biotechnology Co., Ltd. (Shanghai, China). CD45 antibody, CD11b antibody, Ly6G antibody, Ly6C antibody, CD3e antibody, CD8a antibody, CD62L antibody, CD86 antibody, CD11c antibody, F4/80 antibody, CD80 antibody, CD4 antibody, CD25 antibody, Granzyme B antibody, IFN-γ antibody were purchased from Biolegend (San Diego, CA, USA). MHC II antibody, CD206 antibody, CD44 antibody, CD24 antibody were purchased from Elabscience (Wuhan, China).

2.2. Cell lines

The murine breast cancer cells (4T1) and the human breast cancer cells (MDA-MB-231) were obtained from The Cell Bank of the Chinese Academy of Sciences. 4T1 cells and MDA-MB-231 cells were cultured in RPMI-1640 medium with 10% FBS and 1% penicillin-streptomycin (Dalian Meilun Biotechnology, Dalian, China). All cells were cultured at 37 °C in a humidified incubator (Thermo Scientific, 3111, Waltham, USA) with 5% CO_2.

2.3. Animals

All the animal experimental procedures were complied with the institutional ethical guidelines and approved by the Institutional Animal Care and Use Committee (IACUC) of Zhongshan Institute for Drug Discovery. Female BALB/c mice (6−8 weeks old) were purchased from the Zhuhai BesTest Bio-Tech Co., Ltd. (Zhuhai, China). Animals were kept in a facility that was pathogen-free, had free access to food and water, and maintained a 12-h light/dark cycle.

2.4. Orthotopic breast cancer model

The abdomens of the mice were shaved. The mice were anesthetized by isoflurane. Approximately 1×10^6 4T1 cells in 100 μL of PBS were injected orthotopically into BALB/c mouse mammary fat pad through insulin needle, and a cotton swab was then applied to the injection site to prevent leakage of tumor cells.

2.5. Orthotopic breast cancer lung metastasis model

When the orthotopic tumor volume reached about 50 mm^3, approximately 5×10^4 4T1 cells in 100 μL of PBS were intravenously injected into each mouse to develop a lung metastasis model.

2.6. Database

Based on various databases, the bioinformatics analysis was carried out. Differential expression of *PKM* and β-Catenin in normal tissues and breast cancer tumor samples were analyzed based on Breast Cancer Gene-Expression Miner (https://bcgenex.ico.unicancer.fr/BC-GEM/GEM-Chronologie.php), TIMER2.0 database (http://timer.cistrome.org/) and GEPIA (http://gepia.cancer-pku.cn/) database. Based on BEST database (https://rookieutopia.com/app_direct/BEST/) and Kaplan−Meier Plotter database (https://kmplot.com/analysis/), the relationship between *PKM* and β-Catenin expression and prognosis in breast cancer (BRCA) was analyzed. *PKM* and β-Catenin expression in various cell types of tumor tissues was analyzed based on the TISCH database (http://tisch.comp-genomics.org/), specifically in EMTAB8107, GSE110686, GSE114727, GSE148673, GSE161529, and GSE138536 subsets. The correlation of *PKM and* β-Catenin expression in BRCA with macrophages was analyzed based on the TIMER2.0 database. Analysis of *PKM* and β-Catenin expression and immune infiltration in the immune microenvironment of BRCA was performed based on the TCGA database (https://www.cancer.gov/ccg/research/genome-sequencing/tcga).

2.7. Bone marrow-derived MΦ (BMDM) and dendritic cell (BMDC) induction

BALB/c female mice were euthanized and the femur and tibia were then collected, with the muscle removed from the bones. The bones were subsequently immersed in 75% alcohol solution for 10 min and then washed twice with pre-cooled PBS for 5 min each time. The epiphyses were cut at both ends, followed by aspiration of PBS with a syringe to flush the marrow from the bone cavity. The bone marrow cell suspension was transferred to a 15-mL tube and then centrifuged at 2000 rpm for 5 min using a centrifuge (Xiangyi centrifuge Co., Ltd., Hunan, China). Two mililiters of erythrocyte lysate were added to the bone marrow cell precipitate, followed by incubation at room temperature for 5 min, and then centrifuged at 1000 rpm for 5 min using a centrifuge (Xiangyi Centrifuge Co., Ltd.). The bone marrow cells were resuspended in DMEM medium (20% FBS) and cultured for 5 days, with the addition of 20 ng/mL M-CSF to stimulate BMDM differentiation. After that, the medium was changed to 40 ng/mL IL-4-containing DMEM complete media for the induction of BMDM polarization towards M2 by 24-h incubation. To induce BMDM polarization towards M1, 100 ng/mL LPS and 20 ng/mL IFN-γ were added to DMEM complete media and incubated for 24 h. To induce BMDC differentiation, the bone marrow cells were resuspended in DMEM medium (20% FBS) for 4 days, with the addition of 20 ng/mL GM-CSF and 10 ng/mL IL-4. During this period, the semi-adherent cell population was retained by half-exchanging the medium every 48 h.

2.8. The optimum ratio of drugs combination

The optimal drug combination ratio was established by performing CCK8 assay. 4T1 cells were seeded to a 96-well plate (5×10^3 cells/well) and placed in incubator for incubation for 12 h. Then treated with SHK and PTX free or in a series of molar ratios for 24 h. Following the addition of 100 μL of serum-free media containing 10% CCK8 at 37 °C for another 2 h, each well's absorbance (450 nm wavelength) was measured using a microplate reader. Graphpad Prism 8.0.1 (San Diego, CA, USA) was used to determine the IC_{50} values. The combination index (CI) of SHK&PTX was calculated by CompuSyn (CA, USA) software.

Proportions were screened for CI values < 1 at each combined dose. The screened ratios were subsequently administered to mice with orthotopic breast cancer. Briefly, the established orthotopic breast cancer mice were randomly divided into five groups (3 mice

per group), and received saline (control), SHK (5 mg/kg), PTX (10 mg/kg), SHK + PTX (5 mg/kg+ 1 mg/kg, equivalent to at a molar ratio of 1:0.2), SHK + PTX (5 mg/kg + 10 mg/kg, equivalent to at a molar ratio of 1:2), *via* intratumoral injection (q.o.d., 5 times). Tumor volume was closely monitored to evaluate therapeutic efficacy. Mice were deemed dead in accordance with animal welfare regulations, and euthanasia occurred in one of the following situations. Animals were extremely lethargic, with a weight loss of more than 20% compared to the control, or with a tumor size reached 2000 mm^3, or with severe ulceration.

2.9. Preparation and characterization of the albumin nanoparticles (NPs)

The hybrid NPs were created using the high-speed dispersion emulsification-homogenization technique. Briefly, PTX and lecithin were dissolved in absolute ethanol, and SHK was dissolved in DMSO to form the oil phase. Albumin was dissolved in water to constitute the aqueous phase. Once the two phases were combined, the high-speed dispersion machine (IKA, T 25 Digital, Staufen, Germany) was used to generate the primary emulsion. Subsequently, after homogenizing the primary emulsion for ten cycles at a pressure of 12,000 psi, the BSA nanoparticle suspension was prepared using a high-pressure homogenizer (Avestin Inc., EmulsiFlex-B15, Ottawa, Canada). The NPs were purified by a Sephadex™ G-50 (Beijing Solarbio Science&Technology Co., Ltd., S8151, Beijing, China) column.

The dynamic light scattering device (Malvern, Zetasizer Pro, Malvern City, UK) was used to detect the particle size and zeta potential. The particle size change in PBS (pH 7.4) containing 10% neonatal bovine serum and in water at 4 °C was used to gauge the stability of the NPs. HPLC (Agilent, 1260 Infinity II, Santa Clara, USA) was used to assess the drug-loading capacity and encapsulation efficiency, and calculated by the formulas as shown in Eqs. (1) and (2):

$$\text{Encapsulation efficiency}\ (\%) = \frac{\text{Weight of encapsulated drug}}{\text{Weight of total added drug}} \times 100 \quad (1)$$

$$\text{Drug loading capacity}\ (\%) = \frac{\text{Weight of encapsulated drug}}{\text{Weight of NP}} \times 100 \quad (2)$$

The HPLC mobile phase of SHK was composed of methanol (65%) and ultra-pure water (35%), and the HPLC mobile phase of PTX was composed of acetonitrile (40%), methanol (25%), and ultra-pure water (35%). Both of them were at a flow rate of 1.0 mL/min. SHK and PTX were isocratic elution by a C18 column (250 mm × 4.6 mm, FLM Scientific Instrument Co. Ltd., Guangzhou, China) at room temperature. The wavelength was 227 nm for PTX and 216 nm for SHK. A traditional dialysis membrane (MWCO 14 kDa) method was used to assess the *in vitro* drug release in PBS (pH 7.4) after 0.5% (*w*/*v*) SDS was added and the mixture was shaken at 37 °C by a thermostatic shaker (Shanghai HerryTech Co., Ltd., Shanghai, China). Released drugs were also measured employing HPLC (Agilent), as previously mentioned, and the cumulative release was computed.

2.10. Cellular uptake efficiency

4T1 cells were seeded to a 12-well plate (1×10^5 cells/well) and placed in incubator to continue incubation for 12 h. The cells were then co-cultured with coumarin 6-labeled nanoparticles. After 2-h co-incubation the fluorescent images were obtained by a fluorescence microscope (Keyence Co., Ltd. BZ-X800LE, Osaka, Japan) and the intracellular fluorescence was detected by a flow cytometer (NovoCyte Quanteon VBYR, Agilent, California, USA).

2.11. In vitro cytotoxicity test

The cytotoxicity of the free drugs and S/P NP was conducted by the CCK8 method according to the previous description (section 2.8). SHK, PTX, SHK&PTX, and S/P NP were applied to the 4T1 cells in a series of concentration gradients, respectively. Graphpad Prism 8.0.1 was employed to estimate the half-maximal inhibitory concentration (IC_{50}).

2.12. ICD, lactate assay and activate immune-related cells

The 4T1 cells were seeded in a 6-well plate for 12 h and then treated with PBS, SHK (1.0 μmol/L), PTX (0.2 μmol/L), SHK&PTX (0.5 μmol/L+0.1 μmol/L), or S/P NP (equal dose with the combination therapy) for 10 h. The supernatant was collected by ELISA kit for HMGB1 detection according to the manufacturer instruction (Chenglin, Beijing, China). The 4T1 cells were collected and co-incubated with calreticulin (CRT) antibody-Alexa Fluor 488 conjugate and corallite 488-conjugated goat anti-rabbit IgG (H + L) for flow cytometry analysis, and the ICD-cells were characterized by FITC positive cells. To quantify ATP level in 4T1 cells, the cells were processed in accordance with the manufacturer's instructions (Beyotime, Shanghai, China). A lactic acid assay kit was utilized to determine the concentrations of lactate in the 4T1 cell culture medium (Jiancheng Bioengineering Co., Ltd., Nanjing, China).

The BMDC cells were induced differentiation as described above. 4T1 cells were seeded in a 12-well plate for 12 h and then treated with PBS, SHK (1.0 μmol/L), PTX (0.2 μmol/L), SHK&PTX (0.5 μmol/L+0.1 μmol/L), or S/P NP (equal dose with the combination therapy) for 10 h. The BMDC cells were co-cultured with the drug-treated 4T1 cells (also its supernatant) in a Transwell device (an aperture of 0.4 μm, Corning, USA) for 24 h. LPS (200 ng/mL) treatment was added as the positive control. CD11c, MHC II, CD80, and CD86 were applied to characterize the mature BMDC through flow cytometry analysis.

2.13. Combination therapy regulation of macrophages

The bone marrow cells were collected, cultured, and induced as mentioned above. After 24-h stimulation, the M2-type BMDM cells were treated with PBS, SHK (1.0 μmol/L), PTX (0.2 μmol/L), SHK&PTX (0.5 μmol/L+0.1 μmol/L), or S/P NP (equal dose with the combination therapy) for 24 h. M1-type BMDM cells were used as a control group. F4/80, CD86, and CD206 were applied to characterize the phenotype of BMDM through flow cytometry analysis.

2.14. Scratch assay

The 4T1 cells were seeded in a 12-well plate with 8×10^5 cells/well for 12 h and scratched with a 200 μL pipette tip. The cells were then washed with sterile PBS and treated with PBS, SHK (1.0 μmol/L),

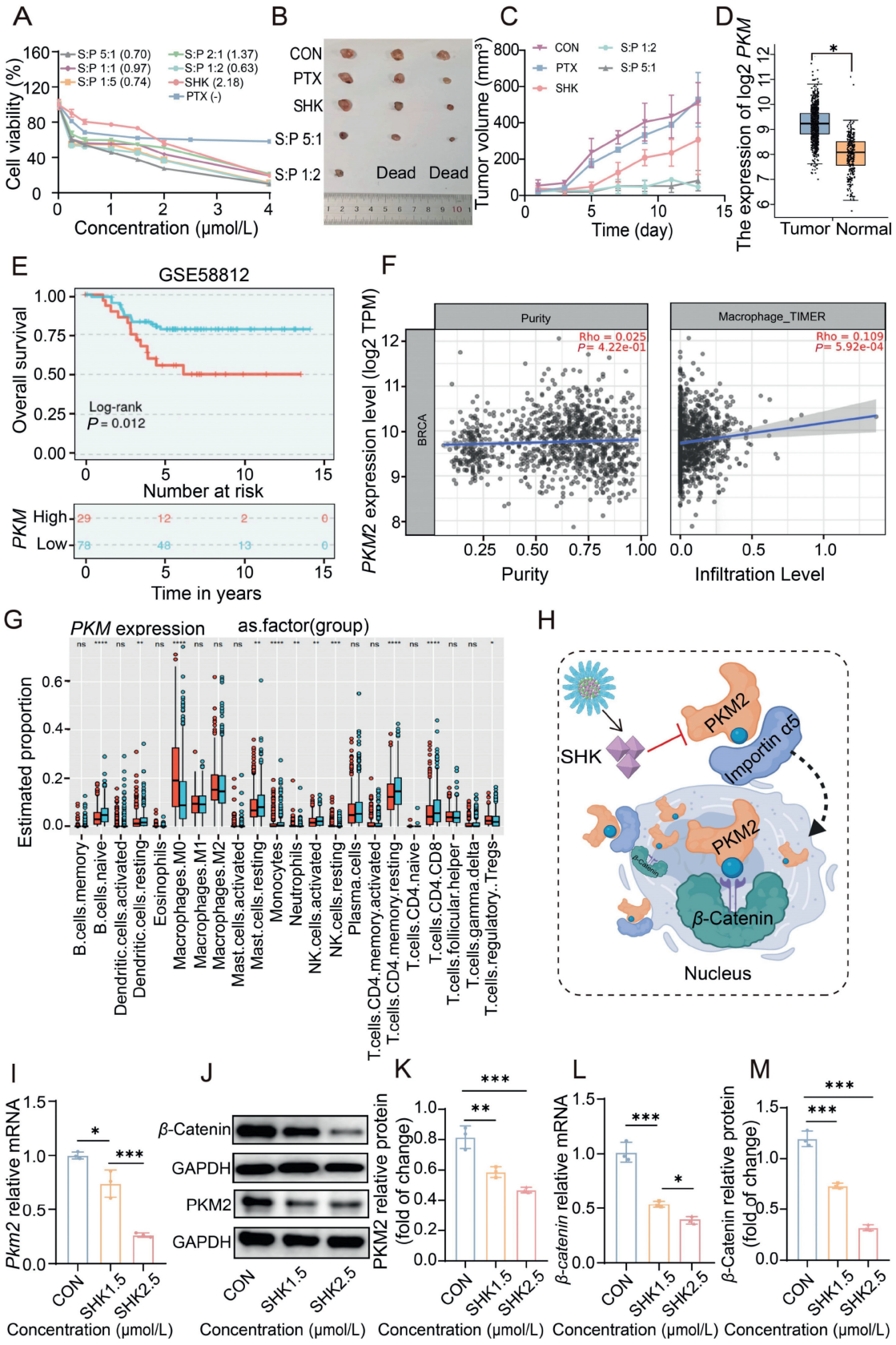

Figure 1 Optimization of drug combination and the high expression of PKM2 in BC. (A) The viability of 4T1 cells under the different combination ratios (SHK: PTX). The value in parentheses is IC_{50} (μmol/L); (B) The dissected tumors at the endpoint under the different combination ratios (SHK: PTX); (C) The tumor volume curves during the treatment; (D) BC tissues overexpressed *PKM2* mRNA compared to normal tissues in the GEPIA database; (E) Correlation analysis between the differential expression of *PKM2* and the overall survival of patients

PTX (0.2 μmol/L), SHK&PTX (0.5 μmol/L+0.1 μmol/L), or S/P NP (equal dose with the combination therapy) for 24 h in the serum-free 1640 medium. The same site was selected and photographed using a microscope (Olympus, IX73P1F, Tokyo, Japan) at 0 and 24 h after drug administration, respectively.

2.15. Matrigel invasion assay

The matrigel invasion assay was evaluated using a Transwell device (an aperture of 8.0 μm, Corning, USA). Firstly, the upper chamber in a Transwell plate was coated with 100 μL matrigel (matrigel:serum-free 1640 medium 1:8), and then the plate was incubated in a 37 °C incubator for 1 h. After that, 75 μL 4T1 cells (4×10^5 cells/well) with 75 μL drugs (PBS, terminal concentration SHK 1.0 μmol/L, PTX 0.2 μmol/L, SHK&PTX 0.5 μmol/L +0.1 μmol/L, or S/P NP equal dose with the combination therapy) and with 5% FBS were seeded into the upper chamber. The lower chamber was filled with 600 μL 1640 medium containing 20% FBS. After 24 h, the upper chamber was washed twice with PBS, followed by formaldehyde fixation for 30 min. The invasion cells in the bottom of the upper chamber were dyed with 0.5% purple crystal and washed with PBS. The image figures were obtained by an inverted microscope.

2.16. Anti-angiogenesis assay

The anti-angiogenesis was evaluated with lactate addition. Briefly, 100 μL of matrigel per well was added to a pre-cooled 96-well plate, and then the plate was incubated in a 37 °C incubator for 1 h. After that, 40 μL 4T1 cells (3×10^4 cells/well) were seeded into the plate containing 10 μL lactate (final concentration of 10 mmol/L), and 50 μL drug (PBS, terminal concentration SHK 1.0 μmol/L, PTX 0.2 μmol/L, SHK&PTX 0.5 μmol/L+0.1 μmol/L, or S/P NP equal dose with the combination therapy). The 4T1 cell tube formation was observed by a microscope in the bright field.

2.17. Tumorsphere destruction

The 4T1 cells were seeded in a 6-well plate for 12 h and then treated with PBS, SHK (1.0 μmol/L), PTX (0.2 μmol/L), SHK&PTX (0.5 μmol/L+0.1 μmol/L), or S/P NP (equal dose with the combination therapy) for 24 h. The serum-free suspension culture was utilized to foster the tumorsphere of 4T1 cells. After trypsinization, the drug-treated adherent cells were cultivated in DMEM/F12 media with the addition of B27 supplement (1 ×), insulin (5 μg/mL), epidermal growth factor (20 ng/mL), basic fibroblast growth factor (20 ng/mL) and then seeded in the 6-well ultra-low attachment plate at 37 °C in a humidified incubator with 5% CO_2, respectively. After 8−12 days, the growth of tumorspheres was observed under a microscope and photographed, and the diameter larger than 50 μm was counted and the average diameter was calculated.

2.18. Flow cytometric detection of cell stemness

The cells were washed twice with phosphate-buffered saline (PBS) and then harvested using 0.05% trypsin/0.025% EDTA. The detached cells were resuspended in 1% BSA at a concentration of 10^6 cells/100 μL. Combinations of CD44 and CD24 antibodies were added to the cell suspension at the concentrations recommended by the manufacturer's instructions and incubated at 4 °C in the dark for 40 min. The labeled cells were then washed with PBS and analyzed using a flow cytometer.

2.19. In vivo distribution

The free Cy5.5 and Cy5.5-labeled S/P NP were intravenously administered into the established mice bearing orthotopic breast tumors, and the IVIS imaging system (PerkinElmer Instruments Co., Ltd., Spectrum, MA, USA) was utilized to monitor the biodistribution of free Cy5.5 and Cy5.5-labeled S/P NP. The mice were humanely euthanized 24 h after injection, and the tumor, heart, liver, spleen, lung, and kidney were collected for *ex vivo* imaging. The distribution of Cy5.5 in tumor tissues was measured by a flow cytometer.

2.20. Establishment of orthotopic model of breast cancer

The 4T1 orthotopic tumor mice were randomly assigned into three groups (6 mice per group). The mice were treated with saline (control), SHK&PTX (2 mg/kg+1.25 mg/kg, equal to SHK:PTX = 5:1, mol/mol), or S/P NP (equivalent to a dose of free drug) *via* tail vein injection (a treatment every 4 days, 4 times). The body weight and the tumor growth were monitored every 3 days throughout the experiment. The tumor volume was calculated according to the formula as shown in Eq. (3):

$$\text{Tumor volume} = \frac{\text{Long diameter} \times (\text{short diameter})^2}{2} \quad (3)$$

All the mice were humanely euthanized to collect the tumor tissues and were weighted to calculate the tumor inhibition ratio (%) according to the formula as shown in Eq. (4):

$$\text{Tumor inhibition ratio}\,(\%) = (1 - W / W_0) \times 100\% \quad (4)$$

W is the tumor weight of the free drug and S/P NP-treated group. W_0 is the tumor weight of the saline-treated group. In order to prepare the single-cell solution, the tumor tissues were physically cut and processed using collagenase IV and hyaluronidase. After incubation with antibodies (CD45 antibody, CD11b antibody, Ly6G antibody, Ly6C antibody, CD3e antibody, CD8a antibody, CD62L antibody, CD86 antibody, CD11c antibody, F4/80 antibody, CD80 antibody, CD4 antibody, CD25 antibody, Granzyme B antibody, IFN-γ antibody, MHC II antibody, CD206 antibody, CD44 antibody), the immune cell subsets in the tumor tissues were analyzed by a flow cytometer.

with BC (Data collected from BEST database GSE58812 array); (F) The correlations between *PKM2* gene expression and macrophage infiltration in BC in TIMER2.0 database; (G) The correlations between *PKM2* gene expression and immune cell infiltration in BC in TCGA database; (H) Schematic mechanism of SHK enhanced the anti-breast cancer effect of PTX; (I, L) The regulatory effect of SHK on the expression of *Pkm2* mRNA and β-catenin mRNA in 4T1 cells; The regulatory effect (J, K, M) of SHK on the expression of PKM2 and β-catenin proteins in 4T1 cells. Data are presented as mean ± SD ($n = 3$). *$P < 0.05$, **$P < 0.01$, ***$P < 0.001$.

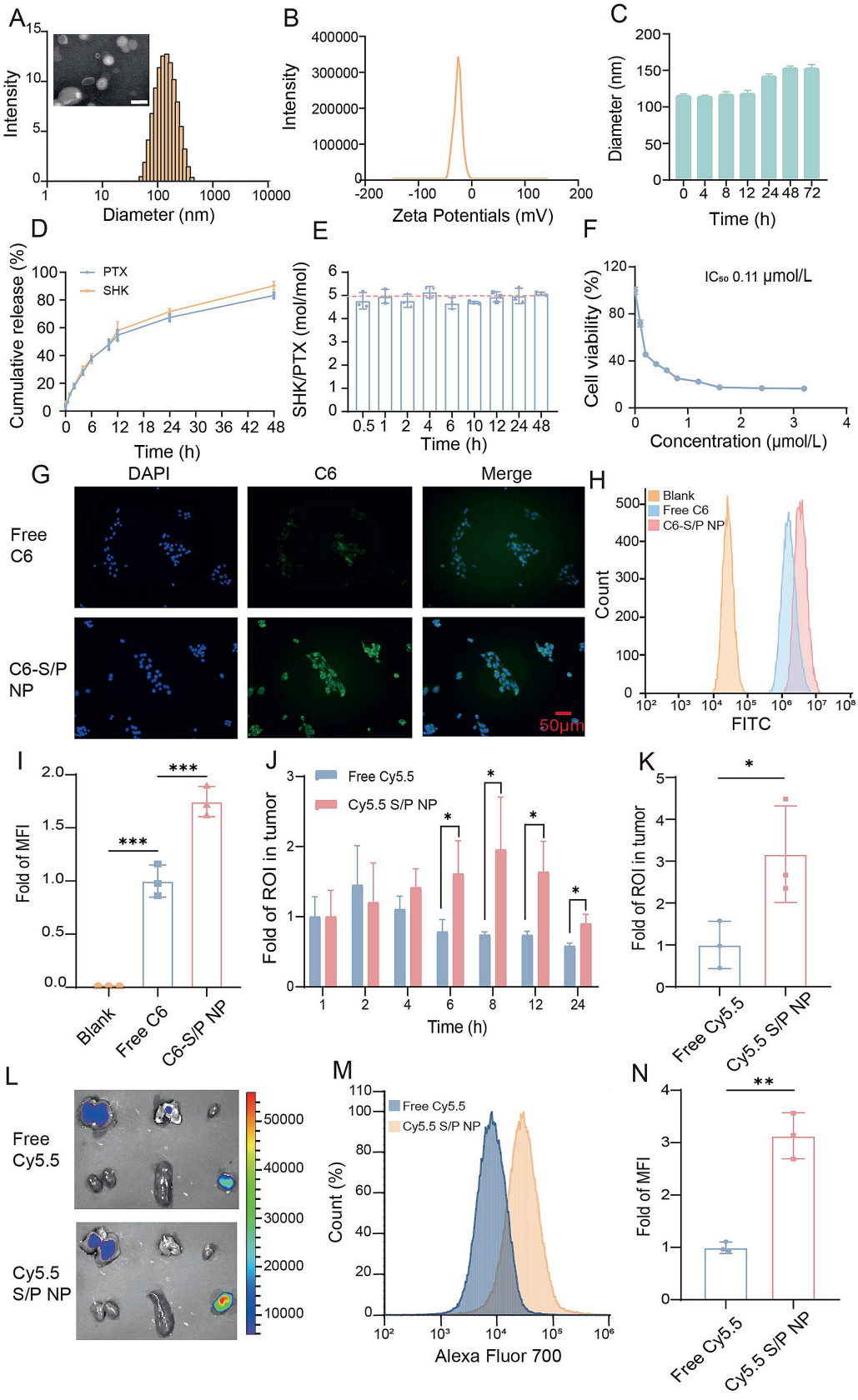

Figure 2 Characterization, cellular uptake and *in vivo* distribution of the nanoparticles. (A) The particle size distribution and the morphological observation with TEM, scale bar = 100 μm; (B) The zeta potential of S/P NP; (C) The stability of S/P NP in serum-containing PBS; (D) *In vitro* release profiles of SHK and PTX from the NP; (E) Cumulative drug release ratios; (F) The cytotoxicity test in 4T1 cells; (G) The inverted

2.21. Establishment of lung metastasis model of orthotopic breast cancer

The 4T1 orthotopic tumor mice were randomly assigned into three groups (6 mice per group). The mice were treated with saline (control), SHK&PTX (2 mg/kg+1.25 mg/kg, equal to SHK:PTX = 5:1, mol/mol), or S/P NP (equivalent to a dose of free drug) *via* tail vein injection (a treatment every 4 days, 6 times). The body weight and the tumor growth were monitored throughout the experiment. The tumor volume was calculated as described above. The blood samples were collected from the animals and plasma was isolated *via* centrifugation for biochemical analysis of aspartate aminotransferase (AST), alanine aminotransferase (ALT), and creatinine (CRE). All the mice were euthanized to collect the tumor tissues and the major organs (heart, liver, spleen, lung, and kidney). In order to further evaluate the system toxicities and visualize the number of pulmonary metastatic nodules, the organs were preserved with 4% paraformaldehyde for histological examination. The tumor tissues were homogenized. The expression levels of the target proteins were determined by Western blot. The PAS/CD31 staining was conducted to estimate the VM.

2.22. Statistical analysis

All data are represented as mean ± standard deviation (SD, $n \geq 3$) with statistical analysis. The semi-quantitative analysis of Western blot bands was conducted by ImageJ software (NIH, USA). Statistical significance was performed by Student's *t*-test or one-way ANOVA (*$P < 0.05$, **$P < 0.01$, and ***$P < 0.001$).

3. Results

3.1. The optimum ratio of drug combination

The anti-proliferative effects on the 4T1 cells and the MDA-MB-231 cells were measured to optimize the combination ratio of SHK and PTX. The combination index (CI) of SHK and PTX was utilized to evaluate the combination therapy efficacy, and CI < 1 indicates the synergistic effect[35]. The synergistic ratio of SHK and PTX in the 4T1 cells was 1:0.2 and 1:2 (mol/mol), with CIs <1 at all doses and the lowest CI was up to 0.21 (SHK:PTX = 1:0.2) and 0.22 (SHK:PTX = 1:2), respectively (Fig. 1A, Supporting Information Fig. S1). Moreover, the most effective synergistic ratio of SHK and PTX in the MDA-MB-231 cells was 1:0.2 (mol/mol) with the lowest CI was up to 0.18 (Supporting Information Fig. S2). Furthermore, in an orthotopic 4T1 BC model, both synergistic ratio treatments achieved a significantly higher tumor inhibition ability compared to the SHK or PTX alone groups (Fig. 1B and C). However, the body weight declined remarkably in the group (SHK:PTX = 1:2) (Supporting Information Fig. S3), suggesting the potential side toxicity. By contrast, the animals maintained their body weight during the treatment of SHK:PTX = 1:0.2, indicating the biosafety. Therefore, a synergistic ratio of 1:0.2 (SHK:PTX) was selected for further studies.

3.2. Bioinformatics analysis of PKM2 and β-Catenin

PKM2 is highly expressed in various cancers and closely associated with reduced efficacy of chemotherapeutics[36]. Therefore, *via* suppression of PKM2, we hypothesized that SHK could enhance PTX efficacy. First of all, we performed a bioinformatics analysis, which demonstrated that *PKM2* expression is higher in the breast tumors and TNBC than in the normal areas (Fig. 1D, Supporting Information Figs. S4 and S5) and overall survival (OS) is much longer in cases of low *PKM2* than in patients with high *PKM2* both in BC and TNBC patients (Fig. 1E, Supporting Information Fig. S6). Recurrence free survival (RFS) is negatively correlative to *PKM2* expression in BC patients, too (Supporting Information Fig. S7). Furthermore, by examining the results of scRNA-seq in multiple datasets, *PKM2* was found to be expressed in several immune cells, with macrophages exhibiting the highest levels of *PKM2* in BC patients (Supporting Information Fig. S8). Moreover, intratumoral *PKM2* expression was positively connected with the increased infiltration of macrophages in both BC and TNBC tumor microenvironment (TME) and it also increased with the purity of the tumor cells in the tumors (Fig. 1F and G, Supporting Information Fig. S9). In addition, *PKM2* expression was positively related to the increased infiltration of Tregs in BC patients (Fig. 1G).

Notably, PKM2 plays a dual role, serving as a glycolytic enzyme in cytoplasm in a tetramer form and as a non-metabolizing enzyme *via* entering the nucleus in a dimer form and triggering the transcription factors[27]. As a case in point, the dimer PKM2 triggers β-Catenin transactivation (Fig. 1H), which subsequently promotes the stemness of cancer cells[37], VM formation[38], and poor chemotherapy efficacy[39]. The qPCR and WB results verified that SHK effectively inhibited the mRNA and protein expression of PKM2 in a dose-dependent manner (Fig. 1I−K). Similarly, we also conducted a bioinformatics analysis of β-Catenin, which was higher both in the BC and TNBC tissues than that in normal tissues (Supporting Information Figs. S10 and S11) and negatively correlative to OS (Supporting Information Figs. S12 and S13). Moreover, β-Catenin was also expressed on the intratumoral macrophages, endothelial cells, and fibroblasts (Supporting Information Fig. S14). Furthermore, β-Catenin high expression was positively correlated with infiltration of naïve B cells, M2 macrophages, and resting DCs and memory $CD4^+$ T cells in TME (Supporting Information Fig. S15).

More importantly, the wet experiment also demonstrated that SHK significantly suppressed β-Catenin in a dose-dependent manner (Fig. 1J, L and M). Taken together, PKM2/β-Catenin might be a crucial signaling pathway for SHK in enhancing the anticancer effect of PTX in BC and TNBC.

3.3. Characterization, cellular studies and in vivo imaging performance of the nanoparticles

SHK and PTX were successfully encapsulated in albumin nanoparticles (S/P NP). The S/P NP showed a spherical morphology and the particle size was about 133 nm (PDI<0.20) (Fig. 2A, Supporting Information Table S1). The S/P NP displayed a negative

microscope image of uptake of S/P NP in 4T1 cells, scale bar = 50 μm; (H, I) The cellular uptake was detected by flow cytometry and statistical analysis of mean fluorescence intensity; (J) The tumors radiant efficiency *in vivo* at different time points; (K) The radiant efficiency semi-quantitative analysis in tumor tissue; (L) *Ex vivo* images of the tumor tissues and major organs (heart, liver, spleen, lung and kidney); (M, N) The $Cy5.5^+$ proportion of the tumors was analyzed by flow cytometry and statistical analysis. NP: Nanoparticles. Data are presented as mean ± SD ($n = 3$). *$P < 0.05$, **$P < 0.01$, ***$P < 0.001$.

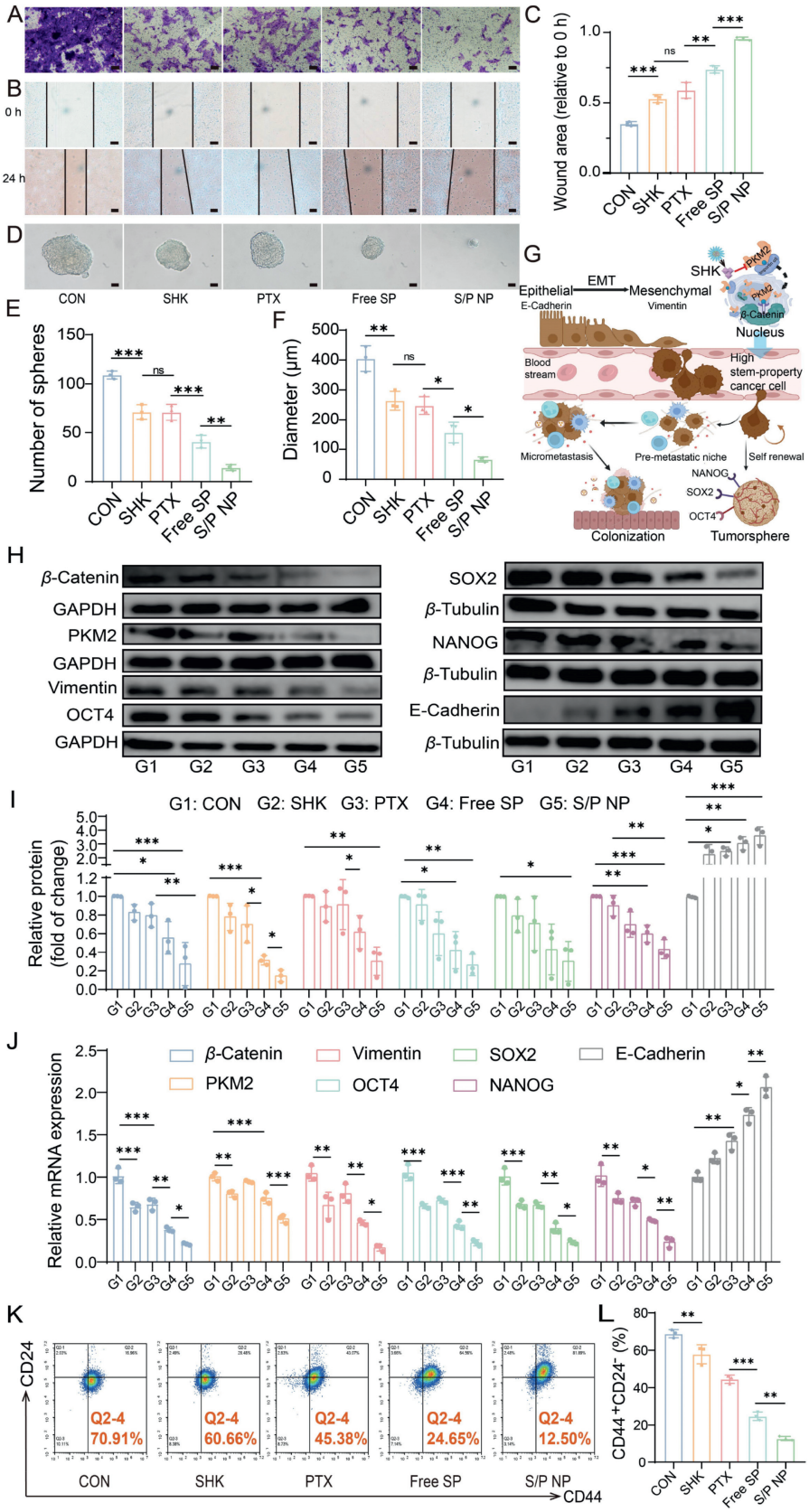

Figure 3 Regulation of the stem-property in 4T1 cells. (A) Transwell analysis in 4T1 cells, scale bars = 200 μm; (B, C) The representative images of scratch assay in 4T1 cells and the statistical analysis of wound area, scale bar = 100 μm; (D) Representative images of the 4T1 tumorspheres on Day 12 after different treatments, scale bar = 50 μm; (E, F) The statistical analysis of number and diameter of tumorspheres; (G) Schematic mechanism of SHK inhibiting stem-property of 4T1 cells; (H) Western blot analysis of PKM2, β-Catenin, epithelial or mesenchymal

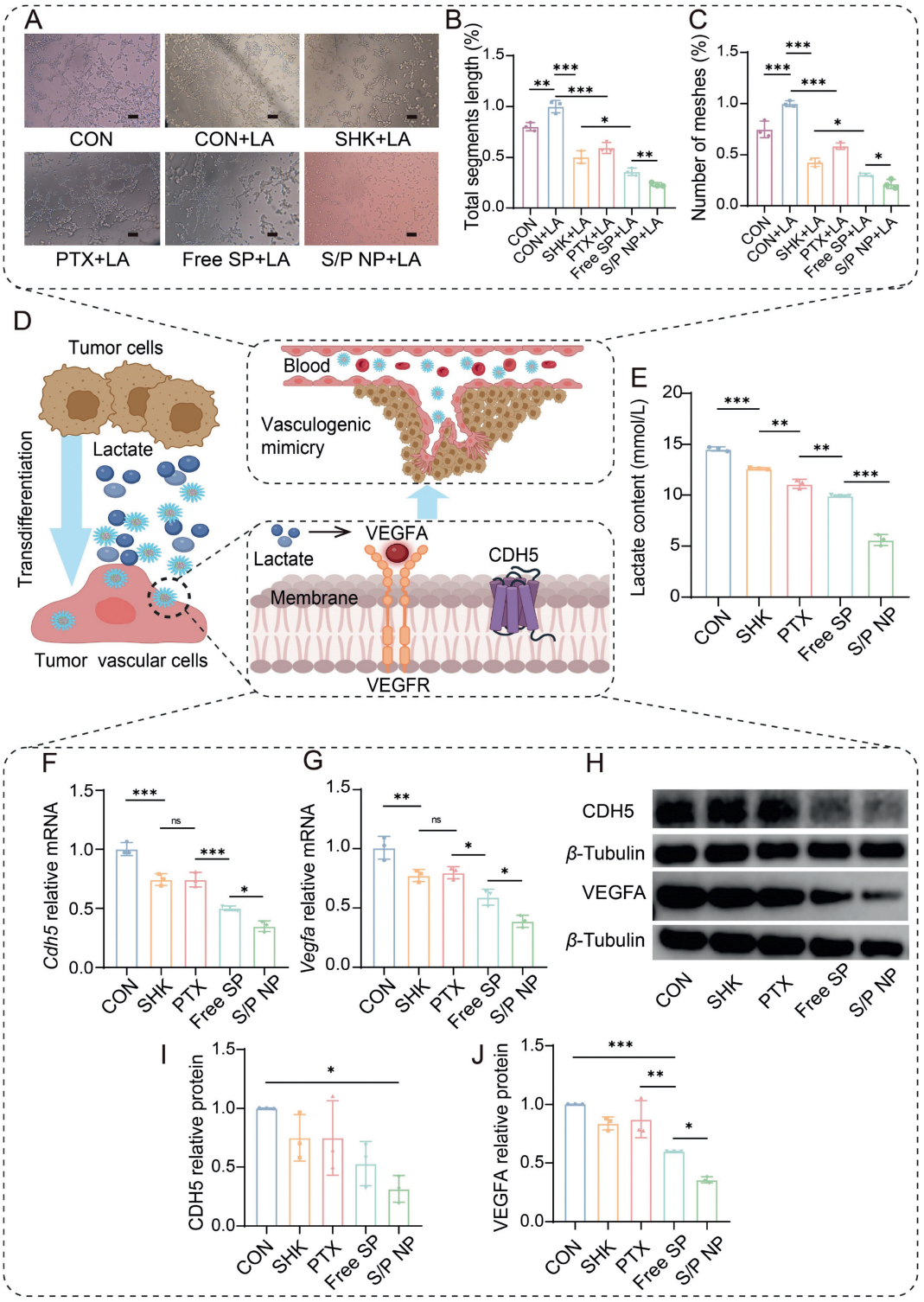

Figure 4 Regulation of the vasculogenic mimicry in 4T1 cells. (A, B) The representative images of tube formation after lactate treatment in 4T1 cells and the statistical analysis of total segments length, scale bar = 100 μm; (C) The statistical analysis of number of meshes; (D) Schematic mechanism of tumor cell vasculogenic mimicry; (E) Quantitative of exocellular lactate of 4T1 cells treated with nanoparticles; The mRNA levels of *Cdh5* (F), *Vegfa* (G) in 4T1 cells; Western blot analysis (H) and quantization (I, J) for CDH5 and VEGFA proteins in 4T1 cells. Data are presented as mean ± SD ($n = 3$). $^{*}P < 0.05$, $^{**}P < 0.01$, $^{***}P < 0.001$, ns, not significant.

markers, stem-property markers in 4T1 cells; Quantization of Western blot analysis (I) and the mRNA levels (J) of β-catenin, *Pkm2, Vimentin, Oct4, Sox2, Nanog* and E-cadherin in 4T1 cells; (K, L) The population of $CD44^{+}/CD24^{-}$ subtype in drug treated 4T1 cells and statistical analysis. Data are presented as mean ± SD ($n = 3$). $^{*}P < 0.05$, $^{**}P < 0.01$, $^{***}P < 0.001$, ns, not significant.

zeta potential about −26 mV (Fig. 2B and Table S1). The SHK- or PTX-loading capacity was 1.39% and 0.89%, respectively, at a drug loading ratio was about 5:1 (SHK:PTX, mol/mol, equal to SHK:PTX 1.6:1, mg/mg) (Table S1). The S/P NP remained stable at 4 °C (Supporting Information Fig. S16) with only a slight increase in size when placed in serum-containing medium, likely due to interactions with blood proteins that form protein coronas (Fig. 2C). The S/P NP showed a drug release pattern at a ratio around 5:1 (SHK:PTX, mol/mol) (Fig. 2D and E).

The combination of SHK/PTX (5:1, mol/mol) displayed a synergistic effect with an IC_{50} of 0.70 μmol/L (indicated by SHK), compared to 2.18 μmol/L for SHK, while the 4T1 cells showed substantial resistance to PTX (Fig. 1A). The S/P NP showed the strongest inhibitory effect with an IC_{50} of 0.11 μmol/L (Fig. 2F).

The Coumarin-6-labeled S/P NP exhibited an efficient internalization in 4T1 cells with a 1.8-fold higher efficiency than the free dye (Fig. 2G–I). Following the approach used in other studies, we chose the Cy5.5 fluorescent dye to assess the targeting ability of the S/P NP[32,40-42]. *In vivo* imaging results showed that the Cy5.5-labeled NPs efficiently accumulated in the tumor after 6 h and reached a maximum at 8 h (Fig. 2J, Supporting Information Fig. S17). The *ex vivo* imaging showed that intratumor accumulation of the NP group was 3-fold higher than the free dye group (Fig. 2K and L), while these two groups showed a similar distribution in the normal organs (Fig. 2L, Supporting Information Fig. S18). Flow cytometric assay also revealed that the intracellular fluorescence intensity was also higher in the NP group (Fig. 2M and N).

3.4. Regulation of the stemness and vasculogenic mimicry (VM) in 4T1 cells

The stemness of tumor cells is an important indicator for assessing the characteristics of self-renewal, differentiation, and proliferation of CSCs[43]. Our results showed that the S/P NP had the highest inhibition rates against invasion and migration of 4T1 cells (Fig. 3A–C). The S/P NP efficiently suppressed the formation of tumor spheroids (Fig. 3D–F). The inhibitory effect of S/P NP on tumor stemness is due to the effects of SHK (Fig. 3G). Moreover, the S/P NP-treated 4T1 cells showed downregulation in the expression of the typical stem-property associated transcription factors including OCT4, NANOG, and SOX2 (Fig. 3H–J). The flow cytometry revealed that after S/P NP treatment, the proportion of high stem-property cell ($CD44^+/CD24^-$) decreased (Fig. 3K and L). Epithelial−mesenchymal transition (EMT) is an index to evaluate the stem-property of cancer cells[44]. Our results showed that the S/P NP treatment led to upregulation of E-Cadherin and downregulation of Vimentin in 4T1 cells, demonstrating the strong ability to reverse EMT (Fig. 3H–J). These results suggested that the S/P NP significantly reduced the stem-property of 4T1 cells. Furthermore, we also detected the protein and mRNA expression of PKM2 and β-Catenin, the S/P NP exhibited the remarkable down-regulation of PKM2 and β-Catenin (Fig. 3H–J).

Distinct from tumor angiogenesis, VM refers to a vasculature network formed by aggressive, plastic tumor cells independent of endothelial cells, and provides a blood supply for tumor cells[16]. CSCs have a higher potential for developing into VM because of their propensity for self-renewal and multidirectional differentiation[22]. Our results revealed that the S/P NP treatment significantly inhibited the tube formation of 4T1 cells (Supporting Information Fig. S19). Lactate is a primary end product of glycolysis, contributing to the acidic TME[45]. Lactate can facilitate the survival of tumor cells by acting as an energy source, while also promoting the formation of vasculature network by tumor cells[46]. After adding lactate, tube formation rate was effectively upregulated (up to 1.3-fold of non-lactate added group), because lactate is a potent angiogenesis inducer. The S/P NP significantly weakened the ability of tube formation in 4T1 cells (Fig. 4A–C). It was attributed to the suppression of lactate production (Fig. 4D and E). Notably, the S/P NP downregulated the mRNA and protein of VM-associated transcription factors including CDH5 and VEGFA (Fig. 4F–J). Taken together, these results indicated that the S/P NP efficiently inhibited the formation of vasculature network of the tumor cells *via* blocking the CDH5/VEGFA pathway and reducing lactate production, thus yielding anti-VM effect.

3.5. Immunogenic cell death (ICD) induction and immunoactivation

The ICD effect triggers DAMPs that are characterized by calreticulin (CRT) eversion, the release of high mobility group box 1 (HMGB-1) and adenosine triphosphate (ATP)[47]. Our results demonstrated the ICD effect induced by the S/P NP, showing CRT eversion by flow cytometry (Fig. 5A and B), HMGB-1 and ATP release to supernatant in the 4T1 cells (Fig. 5C and D).

Tumor-associated macrophages (TAMs) are a promising target for BC therapy[48]. The S/P NP dramatically reduced the proportion of $CD206^+$ MΦ (protumor M2-like subset) (Fig. 5E and F). DCs connect innate immunity and adaptive immunity by presenting antigens to naïve T cells and thereby triggering T cell immunity[49]. In a co-culture system (Fig. 5G), Our results showed that the S/P NP-treated 4T1 cells promoted the maturation of BMDCs, with the upregulation of co-stimulatory molecules (CD80, CD86), indicating the induction of ICD effect in 4T1 cells (Fig. 5H and I).

3.6. Treatment efficacy in a mouse model with orthotopic BC

In an orthotopic 4T1 mouse model (Fig. 6A), the S/P NP effectively arrested tumor growth with an inhibition rate of 80%, compared to 45% of free SHK/PTX (Fig. 6B–D, Supporting Information Fig. S20). The body weight change of the S/P NP group was no significantly different from the control group (Fig. 6E and F).

To profile the remodeled TME, the intratumoral immune cells were detected after treatment. The S/P NP treatment significantly increased the proportion of anti-cancer M1Φ but reducing protumor M2Φ (Fig. 6G and H, Supporting Information Fig. S21). Besides, the percentage of matured DCs was highest in the S/P NP group (Fig. 6I, Supporting Information Fig. S22), while the population of protumoral PMN-MDSCs in the S/P NP group decreased to about 47% of the saline group (Fig. 6J, Supporting Information Fig. S23). These results indicated that the S/P NP treatment effectively relieved the immunosuppression of TME by reprogramming macrophages, promoting DCs maturation, and suppressing PMN-MDSCs. Moreover, the S/P NP treatment significantly promoted memory T cells ($CD62L^+$ $CD44^+$) (Fig. 6K, Supporting Information Fig. S24), suggesting the induction of long-term immune responses. The infiltration of $CD8^+$ T cells was increased (Fig. 6L, Supporting Information Figs. S25A

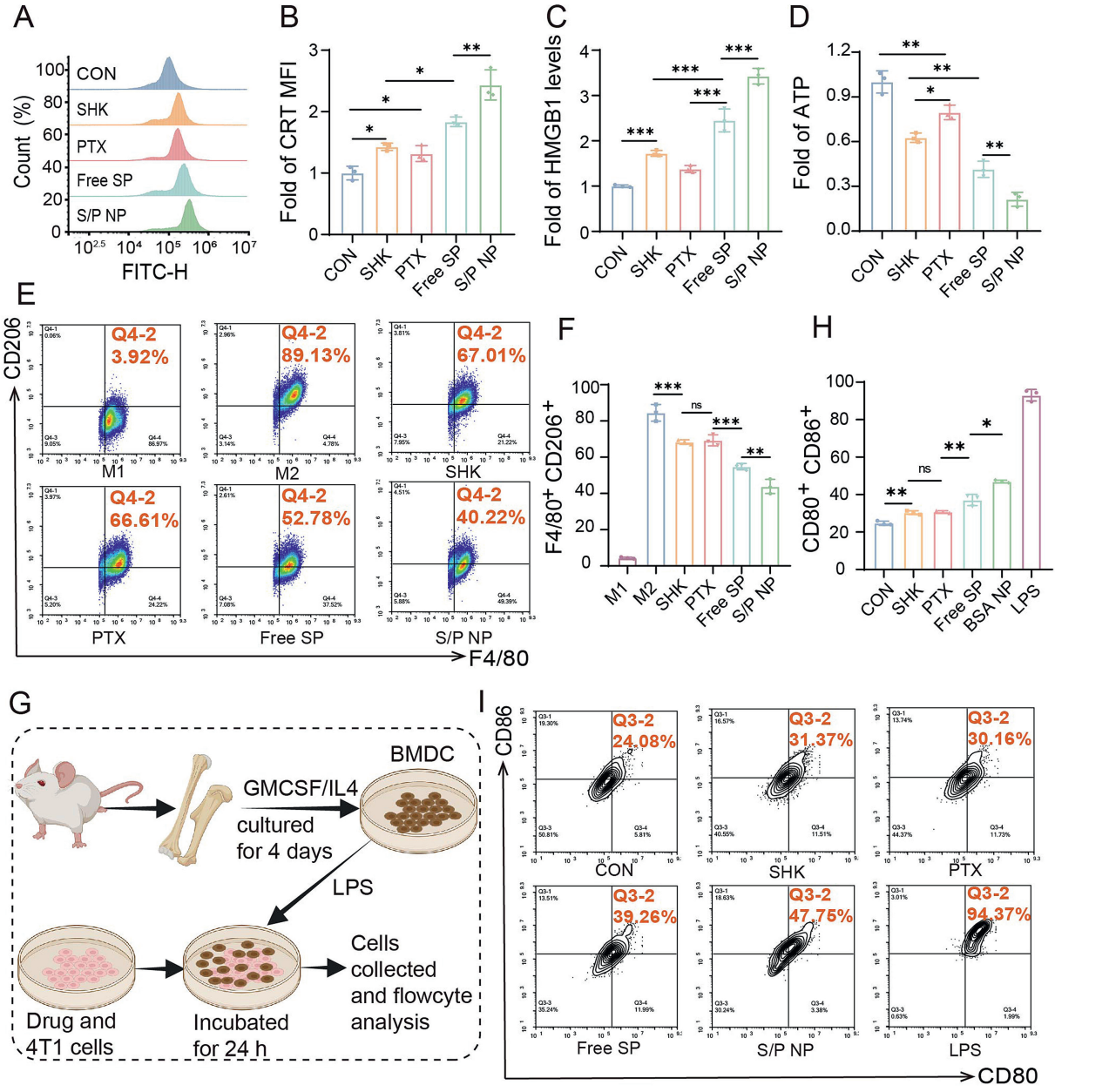

Figure 5 Remodeling of immune microenvironment. (A, B) Analysis of calreticulin (CRT) eversion in 4T1 cells by flow cytometry and statistical analysis; (C) Analysis of the released HMGB-1 of 4T1 cells by ELISA; (D) Quantitative of intracellular ATP of 4T1 cells treated with nanoparticles; (E, F) The population of M2 macrophages after treatment and statistical analysis; (G) Schematic of the ICD stimulated maturation of BMDC; (H, I) The population of matured DC after co-culturing with drug treated 4T1 cells and statistical analysis. Data are presented as mean ± SD ($n = 3$). $^{*}P < 0.05$, $^{**}P < 0.01$, $^{***}P < 0.001$, ns, not significant.

and S25B), and the IFN-γ^+/Granzyme B^+ $CD8^+$ T cell subsets were also significantly expanded (Fig. 6M and N, Fig. S25C and S25D). In addition, we detected the percentage of Treg cells, however, there was no statistical difference among the groups (Supporting Information Fig. S26). The discrepancy could be due to the difference between animal model and human, but further investigation should be carried out for better understanding this. These results confirmed that the S/P NP treatment effectively relieved the immunosuppression of TME and activated T cells immunity against breast tumor.

3.7. Therapeutic efficacy in a mouse model with lung metastasis of orthotopic BC

There are common cases of lung metastasis of advanced BC. The therapeutic efficacy of the S/P NP was evaluated in a lung metastasis mouse model bearing orthotopic 4T1 (Fig. 7A). The S/P NP not only successfully inhibited the progression of primary breast tumor (Fig. 7B and C), but also effectively minimized the lung metastasis nodules with an inhibition rate of 86%, compared to 50% of the free SHK/PTX group (Fig. 7D–F, Supporting

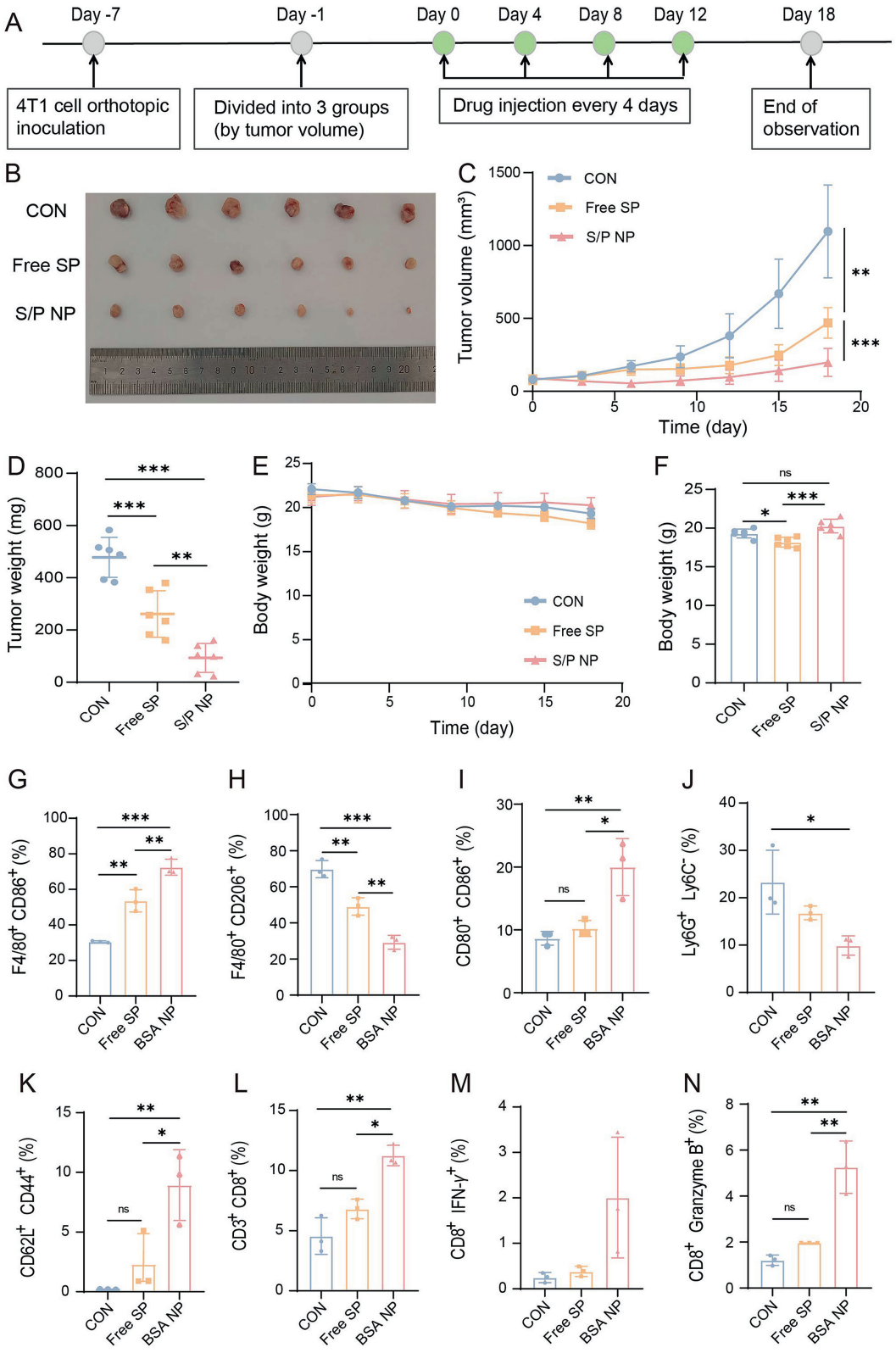

Figure 6 *In vivo* therapeutic efficacy of nanoparticles in a mouse model with orthotopic breast cancer. (A) Therapeutic schedule; (B) The tumor image, (C) tumor volume curves and (D) tumor weight, (E) Body weight curves; (F) Statistical analysis of body weight on the last day during treatment; (G) The ratio of the M1-like TAM ($F4/80^+$ $CD86^+$) subset; (H) The ratio of the M2-like TAM ($F4/80^+CD206^+$) subset; (I) The ratio of the matured DC ($CD80^+CD86^+$) subset; (J) The ratio of the PMN-MDSC ($Ly6G^+Ly6C^-$) subset; (K) The ratio of the memory T cells ($CD62L^+CD44^+$) subset; (L) The ratio of the $CD8^+$ T cells ($CD3^+CD8^+$) subset; (M, N) The ratio of the cytotoxicity $CD8^+$ T cells (IFN γ^+/ Granzyme B^+) subset. Data are presented as mean ± SD ($n = 3-6$). $^*P < 0.05$, $^{**}P < 0.01$, $^{***}P < 0.001$, ns, not significant.

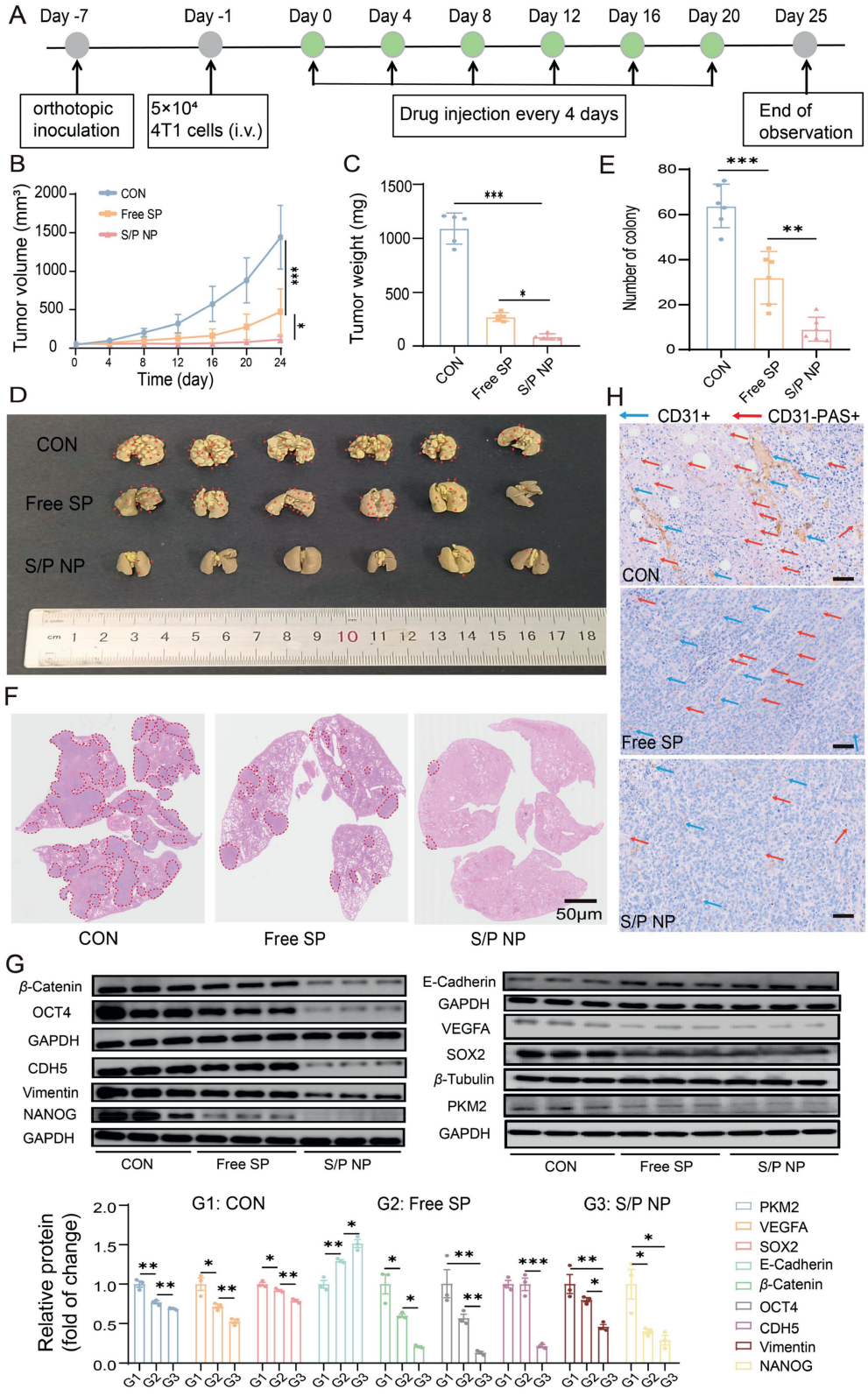

Figure 7 *In vivo* therapeutic efficacy of nanoparticles in a mouse model with lung metastasis of orthotopic BC. (A) Therapeutic schedule; (B) The tumor volume variations and (C) tumor weight; (D, E) The image of lung nodules of groups and the statistical analysis; (F) Representative H&E staining images of the lungs after different treatments (The area circled by the red line represents breast cancer lung metastasis nodules), scale bar = 50 μm; (G) Western blot analysis and quantization of β-Catenin, PKM2, OCT4, SOX2, NANOG, CDH5, VEGFA, Vimentin and E-Cadherin in tumor tissues; (H) Representative CD31/PAS staining of tumor tissue after different treatments. $CD31^+$ represents vascular endothelial cell tube formation. $CD31^-/PAS^+$ represents vasculogenic mimicry, scale bar = 50 μm. Data are presented as mean ± SD (n = 3−6). $^*P < 0.05$, $^{**}P < 0.01$, $^{***}P < 0.001$.

Information Fig. S27). The S/P NP significantly downregulated the expression levels of PKM2, β-Catenin, the stem-property markers SOX2, OCT4, NANOG, VM formation related biotargets CDH5, VEGFA and EMT associated marker Vimentin, while upregulated EMT associated marker E-cadherin (Fig. 7G). Crucially, the PAS/CD31 staining results showed that the S/P NP exhibited a potent inhibitory capacity against VM formation, with the remarkably reduced proportion of $CD31^{-}/PAS^{+}$ (Fig. 7H). These results suggested the regulation of the crosstalk among stem-property and VM contributed to the remission of lung metastasis.

The S/P NP treatment showed a good biosafety in terms of body weight change (Supporting Information Fig. S28). There were also no obvious lesions observed in the H&E staining sections of the organs (Supporting Information Fig. S29). Moreover, no statistically significant difference in ALT, AST, and CRE levels was found among the groups (Supporting Information Fig. S30).

4. Discussion

TNBC patients suffer from poor prognosis, with a median survival time of approximately 4.2 years after diagnosis[50]. PTX is ready to develop drug resistance in TNBC treatment. Hence its combination with other drugs has emerged as a recommended option[6,7]. SHK, one of the main components of *Lithospermum. erythrorhizon*, has been widely investigated in cancer therapy as a PKM2 inhibitor[51]. In our previous report, the glycolysis inhibition effect of SHK was demonstrated, including the down-regulation of PKM2, as well as reduction of ATP and lactate[42,52,53]. Co-delivery systems are commonly employed to overcome the poor efficacy of chemotherapy and improve the *in vivo* delivery of hydrophobic drugs. For example, a co-delivery system of quercetin and doxorubicin, modified with the KC26 peptide, facilitates deep penetration into tumors and strongly inhibits breast tumor growth[54]. In this work, we developed an albumin delivery system (S/P NP) to co-load SHK and PTX in an optimized ratio of 5:1, aiming to enhance the anti-tumor effect of PTX in TNBC.

PKM2 is associated with poor prognosis for patients with cancers and is highly expressed in various malignancies[55], which is in agreement with our results of bioinformatics analysis. PKM2 expression levels were significantly higher in PTX-resistant cancer cells. The upregulated PKM2 contributed to drug resistance by regulating cellular energy metabolism and influencing the stress response of tumor cells[56]. Moreover, PKM2 can affect cellular sensitivity to PTX by modulating mitochondrial function and reactive oxygen species (ROS) production[57]. Therefore, this SHK-based therapeutic strategy can take a dual action for simultaneously inhibiting both glycolysis and β-Catenin signaling pathway, thus synergizing PTX treatment against TNBC by decreasing the stem-property and VM formation, remodeling the TME.

One of the major culprits for unsatisfied outcomes of PTX accounts for the stem-property of TNBC cells which is regulated by the activation of β-Catenin[8]. Meanwhile, the stemness-associated EMT not only causes drug resistance but also promotes tumor metastasis[58,59]. Another mechanism for the ineffectiveness of PTX therapy is VM. There is a correlation between VM and CSCs, and some tumor vessels may originate from the tumor cells through vasculogenesis[60], in which CSCs may act as progenitors of tumor stromal components like tumor vasculogenic stem cells[61]. Furthermore, in the perivascular environment, CSCs primordially grow in VM niches[62], where they transdifferentiate into endothelial-like cells in VM formation. Our results demonstrated that the S/P NP successfully reversed the stem-property and EMT, as well as suppressed VM formation. As a result, the S/P NP significantly enhanced the treatment efficacy of PTX against TNBC and lung metastasis.

TNBC is a typical "cold tumor" with a strong immunosuppressive microenvironment[63]. CSCs are preferentially dispersed in niches with typical TME characteristics[64]. The interaction between CSCs and immune cells in TME often leads to unproductive therapy outcomes[65]. Therefore, targeting CSCs and VM can remodel the tumor immune microenvironment. Our results showed that the S/P NP treatment decreased M2Φ and MDSCs, but promoted M1Φ, matured DCs, CTLs, and memory T cells.

5. Conclusions

In this work, we developed a therapeutic strategy using the S/P NP for targeting the stem-property and VM formation by inhibiting PKM2. This codelivery system enhanced the tumor drug accumulation. Such treatment efficiently arrested the primary tumor growth of TNBC and suppressed lung metastasis.

Acknowledgments

We are thankful for the support from the National Key Research and Development Program of China (2024YFA1210200 and 2022YFE0203600), NSFC (82341232, 82404549, and 82174456, China), the Future Network (083GJHZ2023012FN, China) and Grand Challenges (083GJHZ2023021GC, China) of the International Partnership Program of the Chinese Academy of Sciences, CAS President's International Fellowship Initiative (2024VBB0004, China), the Department of Science and Technology of Guangdong Province (High-level Innovative Research Institute 2021B0909050003, China), and Zhongshan Municipal Bureau of Science and Technology (LJ2021001 & CXTD202201, China), the second batch of social welfare and basic research projects of Zhongshan city (2023B2033, China). This work was also supported by Natural Science Foundation of Shanghai Municipal (24ZR1477500, China). We acknowledge the use of Grammarly and ChatGPT to help review the writing of the manuscript to improve the readability and language. The authors reviewed and edited the content at the final stage and took full responsibility for the content of the publication.

Author contributions

Siqi Wu: Data curation, Formal analysis, Investigation, Writing original draft. Qing Tang: Bioinformatics analysis, Visualization, Methodology, Validation. Weifeng Fang: Visualization, Methodology, Validation. Zhe Sun: Visualization, Methodology, Validation. Meng Zhang: Visualization, Methodology, Validation. Ergang Liu: Project administration, Supervision. Yang Cao: Project administration, Supervision. Yongzhuo Huang: Formal analysis, Project administration, Supervision, Writing – review & editing.

Conflicts of interest

The authors have no conflicts of interest to declare.

Declaration of Generative AI and AI-assisted technologies in the writing process

During the preparation of this work the author used [Grammarly and ChatGPT] in order to [help review the writing of the manuscript to improve the readability and language]. After using this tool, the author reviewed and edited the content as needed and takes full responsibility for the content of the publication.

Appendix A. Supporting information

Supporting information to this article can be found online at https://doi.org/10.1016/j.apsb.2025.04.006.

References

1. Sung H, Ferlay J, Siegel RL, Laversanne M, Soerjomataram I, Jemal A, et al. Global cancer statistics 2020: globocan estimates of incidence and mrtality worldwide for 36 cancers in 185 countries. *CA Cancer J Clin* 2021;**71**:209−49.
2. Leon-Ferre RA, Goetz MP. Advances in systemic therapies for triple negative breast cancer. *BMJ* 2023;**381**:e071674.
3. Schmid P, Adams S, Rugo HS, Schneeweiss A, Barrios CH, Iwata H, et al. Atezolizumab and nab-paclitaxel in advanced triple-negative breast cancer. *N Engl J Med* 2018;**379**:2108−21.
4. Liao L, Zhang YL, Deng L, Chen C, Ma XY, Andriani L, et al. Protein phosphatase 1 subunit PPP1R14B stabilizes STMN1 to promote progression and paclitaxel resistance in triple-negative breast cancer. *Cancer Res* 2023;**83**:471−84.
5. Yu KD, Ye FG, He M, Fan L, Ma D, Mo M, et al. Effect of adjuvant paclitaxel and carboplatin on survival in women with triple-negative breast cancer: a phase 3 randomized clinical trial. *JAMA Oncol* 2020;**6**:1390−6.
6. Emens LA, Adams S, Barrios CH, Diéras V, Iwata H, Loi S, et al. First-line atezolizumab plus nab-paclitaxel for unresectable, locally advanced, or metastatic triple-negative breast cancer: IMpassion130 final overall survival analysis. *Ann Oncol* 2021;**32**:983−93.
7. Fan L, Wang ZH, Ma LX, Wu SY, Wu J, Yu KD, et al. Optimising first-line subtyping-based therapy in triple-negative breast cancer (FUTURE-SUPER): a multi-cohort, randomised, phase 2 trial. *Lancet Oncol* 2024;**25**:184−97.
8. Luo F, Zhang M, Sun B, Xu C, Yang Y, Zhang Y, et al. LINC00115 promotes chemoresistant breast cancer stem-like cell stemness and metastasis through SETDB1/PLK3/HIF1α signaling. *Mol Cancer* 2024;**23**:60.
9. Mai Y, Su J, Yang C, Xia C, Fu L. The strategies to cure cancer patients by eradicating cancer stem-like cells. *Mol Cancer* 2023;**22**:171.
10. Massagué J, Ganesh K. Metastasis-initiating cells and ecosystems. *Cancer Discov* 2021;**11**:971−94.
11. Guo W, Sun YF, Shen MN, Ma XL, Wu J, Zhang CY, et al. Circulating tumor cells with stem-like phenotypes for diagnosis, prognosis, and therapeutic response evaluation in hepatocellular carcinoma. *Clin Cancer Res* 2018;**24**:2203−13.
12. Vipparthi K, Hari K, Chakraborty P, Ghosh S, Patel AK, Ghosh A, et al. Emergence of hybrid states of stem-like cancer cells correlates with poor prognosis in oral cancer. *iScience* 2022;**25**:104317.
13. Treps L, Faure S, Clere N. Vasculogenic mimicry, a complex and devious process favoring tumorigenesis—interest in making it a therapeutic target. *Pharmacol Ther* 2021;**223**:107805.
14. Li XY, Zhao Y, Sun MG, Shi JF, Ju RJ, Zhang CX, et al. Multifunctional liposomes loaded with paclitaxel and artemether for treatment of invasive brain glioma. *Biomaterials* 2014;**35**:5591−604.
15. Maddison K, Bowden NA, Graves MC, Tooney PA. Characteristics of vasculogenic mimicry and tumour to endothelial transdifferentiation in human glioblastoma: a systematic review. *BMC Cancer* 2023;**23**:185.
16. Luo Q, Wang J, Zhao W, Peng Z, Liu X, Li B, et al. Vasculogenic mimicry in carcinogenesis and clinical applications. *J Hematol Oncol* 2020;**13**:19.
17. Morales-Guadarrama G, García-Becerra R, Méndez-Pérez EA, García-Quiroz J, Avila E, Díaz L. Vasculogenic mimicry in breast cancer: clinical relevance and drivers. *Cells* 2021;**10**:1758.
18. Hujanen R, Almahmoudi R, Karinen S, Nwaru BI, Salo T, Salem A. Vasculogenic mimicry: a promising prognosticator in head and neck squamous cell carcinoma and esophageal cancer?. A systematic review and meta-analysis. *Cells* 2020;**9**:507.
19. Yao XH, Ping YF, Bian XW. Contribution of cancer stem cells to tumor vasculogenic mimicry. *Protein Cell* 2011;**2**:266−72.
20. Liu TJ, Sun BC, Zhao XL, Zhao XM, Sun T, Gu Q, et al. $CD133^+$ cells with cancer stem cell characteristics associates with vasculogenic mimicry in triple-negative breast cancer. *Oncogene* 2013;**32**:544−53.
21. Chen J, Chen S, Zhuo L, Zhu Y, Zheng H. Regulation of cancer stem cell properties, angiogenesis, and vasculogenic mimicry by miR-450a-5p/SOX2 axis in colorectal cancer. *Cell Death Dis* 2020;**11**:173.
22. Wei X, Chen Y, Jiang X, Peng M, Liu Y, Mo Y, et al. Mechanisms of vasculogenic mimicry in hypoxic tumor microenvironments. *Mol Cancer* 2021;**20**:7.
23. Dong C, Yuan T, Wu Y, Wang Y, Fan TW, Miriyala S, et al. Loss of FBP1 by Snail-mediated repression provides metabolic advantages in basal-like breast cancer. *Cancer Cell* 2013;**23**:316−31.
24. Zhang J, Ouyang F, Gao A, Zeng T, Li M, Li H, et al. ESM1 enhances fatty acid synthesis and vascular mimicry in ovarian cancer by utilizing the PKM2-dependent Warburg effect within the hypoxic tumor microenvironment. *Mol Cancer* 2024;**23**:94.
25. Hou PP, Luo LJ, Chen HZ, Chen QT, Bian XL, Wu SF, et al. Ectosomal PKM2 promotes HCC by inducing macrophage differentiation and remodeling the tumor microenvironment. *Mol Cell* 2020;**78**:1192−206.e10.
26. Zhu S, Guo Y, Zhang X, Liu H, Yin M, Chen X, et al. Pyruvate kinase M2 (PKM2) in cancer and cancer therapeutics. *Cancer Lett* 2021;**503**:240−8.
27. Yang W, Xia Y, Ji H, Zheng Y, Liang J, Huang W, et al. Nuclear PKM2 regulates β-catenin transactivation upon EGFR activation. *Nature* 2011;**480**:118−22.
28. Zhang Y, Wang X. Targeting the Wnt/β-catenin signaling pathway in cancer. *J Hematol Oncol* 2020;**13**:165.
29. Liu S, Sun Y, Hou Y, Yang L, Wan X, Qin Y, et al. A novel lncRNA ROPM-mediated lipid metabolism governs breast cancer stem cell properties. *J Hematol Oncol* 2021;**14**:178.
30. Ni M, Zhou J, Zhu Z, Xu Q, Yin Z, Wang Y, et al. Shikonin and cisplatin synergistically overcome cisplatin resistance of ovarian cancer by inducing ferroptosis *via* upregulation of HMOX1 to promote Fe^{2+} accumulation. *Phytomedicine* 2023;**112**:154701.
31. Zhao P, Wang Y, Wu A, Rao Y, Huang Y. Roles of albumin-binding proteins in cancer progression and biomimetic targeted drug delivery. *Chembiochem* 2018;**19**:1796−805.
32. Zhao P, Wang Y, Kang X, Wu A, Yin W, Tang Y, et al. Dual-targeting biomimetic delivery for anti-glioma activity *via* remodeling the tumor microenvironment and directing macrophage-mediated immunotherapy. *Chem Sci* 2018;**9**:2674−89.
33. Zhao P, Yin W, Wu A, Tang Y, Wang J, Pan Z, et al. Dual-targeting to cancer cells and M2 macrophages *via* biomimetic delivery of mannosylated albumin nanoparticles for drug-resistant cancer therapy. *Adv Funct Mater* 2017;**27**:1700403.
34. Lin T, Zhao P, Jiang Y, Tang Y, Jin H, Pan Z, et al. Blood−brain-barrier-penetrating albumin nanoparticles for biomimetic drug delivery *via* albumin-binding protein pathways for antiglioma therapy. *ACS Nano* 2016;**10**:9999−10012.
35. Zhao P, Zhang J, Wu A, Zhang M, Zhao Y, Tang Y, et al. Biomimetic codelivery overcomes osimertinib-resistant NSCLC and brain metastasis *via* macrophage-mediated innate immunity. *J Control Release* 2021;**329**:1249−61.

36. Qian C, Zhou Y, Zhang T, Dong G, Song M, Tang Y, et al. Targeting PKM2 signaling cascade with salvianic acid A normalizes tumor blood vessels to facilitate chemotherapeutic drug delivery. *Acta Pharm Sin B* 2024;**14**:2077−96.
37. Huang Q, Liu L, Xiao D, Huang Z, Wang W, Zhai K, et al. $CD44^+$ lung cancer stem cell-derived pericyte-like cells cause brain metastases through GPR124-enhanced trans-endothelial migration. *Cancer Cell* 2023;**41**:1621−36.e8.
38. Delgado-Bellido D, Zamudio-Martínez E, Fernández-Cortés M, Herrera-Campos AB, Olmedo-Pelayo J, Perez CJ, et al. VE-CADHERIN modulates β- catenin/TCF-4 to enhance vasculogenic mimicry. *Cell Death Dis* 2023;**14**:135.
39. Xu X, Yu Y, Zhang W, Ma W, He C, Qiu G, et al. SHP-1 inhibition targets leukaemia stem cells to restore immunosurveillance and enhance chemosensitivity by metabolic reprogramming. *Nat Cell Biol* 2024;**26**:464−77.
40. Yu Y, Li J, Song B, Ma Z, Zhang Y, Sun H, et al. Polymeric PD-L1 blockade nanoparticles for cancer photothermal-immunotherapy. *Biomaterials* 2022;**280**:121312.
41. Cheng Y, Xu M, Wu J, Qian K, Yang P, Zhou L, et al. Carcinoma-astrocyte gap junction interruption by a dual-targeted biomimetic liposomal system to attenuate chemoresistance and treat brain metastasis. *ACS Nano* 2024;**18**:34107−25.
42. Wang H, Tang Y, Fang Y, Zhang M, Wang H, He Z, et al. Reprogramming tumor immune microenvironment (TIME) and metabolism *via* biomimetic targeting codelivery of shikonin/JQ1. *Nano Lett* 2019; **19**:2935−44.
43. Espinosa-Sánchez A, Suárez-Martínez E, Sánchez-Díaz L, Carnero A. Therapeutic targeting of signaling pathways related to cancer stemness. *Front Oncol* 2020;**10**:1533.
44. Romano S, Tufano M, D'Arrigo P, Vigorito V, Russo S, Romano MF. Cell stemness, epithelial-to-mesenchymal transition, and immunoevasion: intertwined aspects in cancer metastasis. *Semin Cancer Biol* 2020;**60**:181−90.
45. Hayes C, Donohoe CL, Davern M, Donlon NE. The oncogenic and clinical implications of lactate induced immunosuppression in the tumour microenvironment. *Cancer Lett* 2021;**500**:75−86.
46. Chen Y, Wu J, Zhai L, Zhang T, Yin H, Gao H, et al. Metabolic regulation of homologous recombination repair by MRE11 lactylation. *Cell* 2024;**187**:294−311.e21.
47. Kroemer G, Galassi C, Zitvogel L, Galluzzi L. Immunogenic cell stress and death. *Nat Immunol* 2022;**23**:487−500.
48. Xiang X, Wang J, Lu D, Xu X. Targeting tumor-associated macrophages to synergize tumor immunotherapy. *Signal Transduct Target Ther* 2021;**6**:75.
49. Cabeza-Cabrerizo M, Cardoso A, Minutti CM, Pereira da Costa M, Reis e, Sousa C. Dendritic cells revisited. *Annu Rev Immunol* 2021;**39**:131−66.
50. Garmpis N, Damaskos C, Garmpi A, Nikolettos K, Dimitroulis D, Diamantis E, et al. Molecular classification and future therapeutic challenges of triple-negative breast cancer. *In Vivo (Athens)* 2020;**34**: 1715−27.
51. Boulos JC, Rahama M, Hegazy MF, Efferth T. Shikonin derivatives for cancer prevention and therapy. *Cancer Lett* 2019;**459**:248−67.
52. Long L, Xiong W, Lin F, Hou J, Chen G, Peng T, et al. Regulating lactate-related immunometabolism and EMT reversal for colorectal cancer liver metastases using shikonin targeted delivery. *J Exp Clin Cancer Res* 2023;**42**:117.
53. Zhu J, Wang R, Yang C, Shao X, Zhang Y, Hou J, et al. Blocking tumor-platelet crosstalk to prevent tumor metastasis *via* reprograming glycolysis using biomimetic membrane-hybridized liposomes. *J Control Release* 2024;**366**:328−41.
54. Zhao P, Wang S, Jiang J, Gao Y, Wang Y, Zhao Y, et al. Targeting lactate metabolism and immune interaction in breast tumor *via* protease-triggered delivery. *J Control Release* 2023;**358**: 706−17.
55. Li T, Han J, Jia L, Hu X, Chen L, Wang Y. PKM2 coordinates glycolysis with mitochondrial fusion and oxidative phosphorylation. *Protein Cell* 2019;**10**:583−94.
56. Samec M, Liskova A, Koklesova L, Samuel SM, Zhai K, Buhrmann C, et al. Flavonoids against the Warburg phenotype-concepts of predictive, preventive and personalised medicine to cut the Gordian knot of cancer cell metabolism. *EPMA J* 2020;**11**:377−98.
57. Wang Z, Yin J, Li M, Shen J, Xiao Z, Zhao Y, et al. Combination of shikonin with paclitaxel overcomes multidrug resistance in human ovarian carcinoma cells in a P-gp-independent manner through enhanced ROS generation. *Chin Med* 2019;**14**:7.
58. Jin H, He Y, Zhao P, Hu Y, Tao J, Chen J, et al. Targeting lipid metabolism to overcome EMT-associated drug resistance *via* integrin beta3/FAK pathway and tumor-associated macrophage repolarization using legumain-activatable delivery. *Theranostics* 2019;**9**: 265−78.
59. Grasset EM, Dunworth M, Sharma G, Loth M, Tandurella J, Cimino-Mathews A, et al. Triple-negative breast cancer metastasis involves complex epithelial-mesenchymal transition dynamics and requires vimentin. *Sci Transl Med* 2022;**14**:eabn7571.
60. Pezzolo A, Parodi F, Corrias MV, Cinti R, Gambini C, Pistoia V. Tumor origin of endothelial cells in human neuroblastoma. *J Clin Oncol* 2007;**25**:376−83.
61. Gao JX. Cancer stem cells: the lessons from pre-cancerous stem cells. *J Cell Mol Med* 2008;**12**:67−96.
62. Lizárraga-Verdugo E, Avendaño-Félix M, Bermúdez M, Ramos-Payán R, Pérez-Plasencia C, Aguilar-Medina M. Cancer stem cells and its role in angiogenesis and vasculogenic mimicry in gastrointestinal cancers. *Front Oncol* 2020;**10**:413.
63. Yi M, Li T, Niu M, Mei Q, Zhao B, Chu Q, et al. Exploiting innate immunity for cancer immunotherapy. *Mol Cancer* 2023;**22**:187.
64. Wu B, Shi X, Jiang M, Liu H. Cross-talk between cancer stem cells and immune cells: potential therapeutic targets in the tumor immune microenvironment. *Mol Cancer* 2023;**22**:38.
65. Maccalli C, Rasul KI, Elawad M, Ferrone S. The role of cancer stem cells in the modulation of anti-tumor immune responses. *Semin Cancer Biol* 2018;**53**:189−200.